Human chimeric antigen receptor macrophages for cancer immunotherapy

Michael Klichinsky[1,2,3], Marco Ruella [1,4], Olga Shestova[1], Xueqing Maggie Lu[1,5], Andrew Best[1,3], Martha Zeeman[3], Maggie Schmierer[3], Konrad Gabrusiewicz[3], Nicholas R. Anderson [3], Nicholas E. Petty[1], Katherine D. Cummins[1], Feng Shen[1], Xinhe Shan [1], Kimberly Veliz [1], Kristin Blouch[1], Yumi Yashiro-Ohtani[3], Saad S. Kenderian[1,8], Miriam Y. Kim[1,9], Roddy S. O'Connor [1], Stephen R. Wallace[1], Miroslaw S. Kozlowski[1], Dylan M. Marchione [2,6], Maksim Shestov[1], Benjamin A. Garcia[6], Carl H. June[1,2,7] and Saar Gill [1,2,4] ✉

Chimeric antigen receptor (CAR) T cell therapy has shown promise in hematologic malignancies, but its application to solid tumors has been challenging[1–4]. Given the unique effector functions of macrophages and their capacity to penetrate tumors[5], we genetically engineered human macrophages with CARs to direct their phagocytic activity against tumors. We found that a chimeric adenoviral vector overcame the inherent resistance of primary human macrophages to genetic manipulation and imparted a sustained pro-inflammatory (M1) phenotype. CAR macrophages (CAR-Ms) demonstrated antigen-specific phagocytosis and tumor clearance in vitro. In two solid tumor xenograft mouse models, a single infusion of human CAR-Ms decreased tumor burden and prolonged overall survival. Characterization of CAR-M activity showed that CAR-Ms expressed pro-inflammatory cytokines and chemokines, converted bystander M2 macrophages to M1, upregulated antigen presentation machinery, recruited and presented antigen to T cells and resisted the effects of immunosuppressive cytokines. In humanized mouse models, CAR-Ms were further shown to induce a pro-inflammatory tumor microenvironment and boost anti-tumor T cell activity.

The solid tumor microenvironment (TME) actively recruits myeloid cells, leading to extensive infiltration with immunosuppressive macrophages[6–8]. Macrophages are abundant in the TME of most cancers, where they promote invasion and angiogenesis, facilitate metastasis and increase immunosuppression[9]. TME macrophages arise primarily from bone marrow-derived monocytes that are recruited by tumor or stroma-derived chemokines[9,10]. The importance of macrophages in the TME has generated interest in therapeutic approaches to deplete immunosuppressive tumor-associated macrophages (TAMs) or enhance macrophage phagocytosis[11–13]. Therapeutic approaches to deplete, repolarize or disinhibit the phagocytic activity of TAMs are in clinical development[11,12,14,15]. Current macrophage-based immunotherapeutic approaches are mechanistically dependent on TAMs, which express both activating

and inhibitory Fc receptors, are polarized toward a pro-tumoral and immunosuppressive (M2) phenotype and lack tumor-associated antigen specificity[16].

Outside the environment of established tumors, macrophages are central effectors and regulators of the innate immune system, capable of phagocytosis, cellular cytotoxicity, secretion of pro-inflammatory factors and antigen presentation to T cells[17]. Macrophages are critical effectors of targeted antibody-based cancer therapy[14], and as professional antigen-presenting cells, activated macrophages can play a role in promoting an adaptive anti-tumor immune response[18–20].

These considerations spurred previous attempts to adoptively transfer high numbers of autologous macrophages to patients with solid tumors[21]. These clinical trials demonstrated the feasibility and safety of infusing up to 3×10^9 autologous monocyte-derived macrophages but failed to demonstrate notable anti-tumor efficacy[21–23]. We hypothesized that the expression of CARs in human macrophages could redirect their phagocytic function and result in a targeted anti-tumor therapeutic effect with the potential to stimulate an adaptive immune response.

To model the potential for CAR-mediated redirection of macrophage phagocytosis, we transduced the human macrophage THP-1 cell line with a first-generation anti-CD19 CAR encoding the CD3ζ intracellular domain. CD3ζ has homology to the Fc common γ-chain, FcεRI-γ, a canonical signaling molecule for antibody-dependent cellular phagocytosis (ADCP) in macrophages. We measured the phagocytic potential of macrophages expressing an intact (CAR19ζ) or a truncated (CAR19Δζ) CAR lacking the CD3ζ intracellular domain (Supplementary Fig. 1a). CAR19ζ but neither CAR19Δζ nor control untransduced (UTD) macrophages phagocytosed antigen-bearing tumor cells in an antigen-specific manner (Fig. 1a,b). CAR-M phagocytosis was an active process requiring Syk, non-muscle myosin IIA and actin polymerization, similarly to Fc receptor-mediated ADCP (Supplementary Fig. 1b). CAR activity was equivalent regardless of the use of CD3ζ and Fcγ-based

[1]Center for Cellular Immunotherapies, University of Pennsylvania School of Medicine, Philadelphia, PA, USA. [2]Department of Systems Pharmacology and Translational Therapeutics, University of Pennsylvania School of Medicine, Philadelphia, PA, USA. [3]Carisma Therapeutics, Philadelphia, PA, USA. [4]Division of Hematology-Oncology, Department of Medicine, University of Pennsylvania School of Medicine, Philadelphia, PA, USA. [5]Institute for Biomedical Informatics, University of Pennsylvania, Philadelphia, PA, USA. [6]Department of Biochemistry and Biophysics, University of Pennsylvania Perelman School of Medicine, Philadelphia, PA, USA. [7]Department of Pathology and Laboratory Medicine, University of Pennsylvania School of Medicine, Philadelphia, PA, USA. [8]Present address: Division of Hematology, Mayo Clinic, Rochester, MN, USA. [9]Present address: Department of Medicine, Oncology Division, Washington University School of Medicine, St. Louis, MO, USA. ✉e-mail: saar.gill@pennmedicine.upenn.edu

signaling domains (Supplementary Fig. 1c), and all subsequent experiments were performed using CD3ζ-based CARs. CAR-mediated macrophage phagocytosis was confirmed by video microscopy (Supplementary Videos 1 and 2 and Supplementary Fig. 1d) and by imaging flow cytometry (Supplementary Fig. 1e). CAR-Ms were capable of polyphagocytosis (representative images, Supplementary Fig. 1f). We next generated CAR-Ms targeting the solid tumor antigens mesothelin or HER2 and demonstrated phagocytosis of antigen-positive target cells (Fig. 1c,d). Together, these data demonstrated that CD3ζ-based CARs can direct anti-tumor phagocytic activity and provided support for subsequent efforts to translate this platform to primary human macrophages.

Gene transfer into primary human macrophages has been a longstanding challenge. Given that macrophages express CD46 (Fig. 1e), the docking protein for group B adenoviruses such as Ad35 (ref. [24]), we evaluated a replication-incompetent chimeric adenoviral vector (Ad5f35)[25] as a method of CAR delivery to macrophages. Primary human macrophages were generated from peripheral blood CD14^{+} monocytes with GM-CSF, as GM-CSF is associated with an M1-prone differentiation status[26]. We engineered an anti-HER2 CAR (Supplementary Fig. 1g) into an Ad5f35 vector and demonstrated that Ad5f35-transduced human macrophages expressed CAR with high efficiency (Fig. 1f) and reproducibility between donors (Fig. 1g). The resultant primary human anti-HER2 CAR-Ms demonstrated antigen-specific phagocytosis of HER2^{+} beads and tumor cells (Fig. 1h,i). CAR-M eradicated SKOV3, a HER2^{+} ovarian cancer cell line, in a dose- and time-dependent manner (Fig. 1j,k). The level of tumor phagocytosis and killing directly correlated with the level of CAR expression (Supplementary Fig. 1h) and with the level of target antigen expression (Supplementary Fig. 1i,j). Notably, macrophages transduced by empty Ad5f35 (containing no transgene) at an equivalent multiplicity of infection (MOI) lacked anti-tumor activity (Supplementary Fig. 1k). To evaluate the potential for on-target, off-tumor toxicity, we evaluated the HER2 expression and anti-HER2 CAR-M phagocytosis of a panel of 20 representative normal human tissues and found that normal cells were not phagocytosed (Supplementary Fig. 2a,b).

We next tested the anti-tumor activity of CAR-Ms in vivo using two distinct models in NOD-scid IL2Rg$_{null}$-3/GM/SF (NSGS) mice[27]. In the first approach, SKOV3 cells were injected intravenously (IV) leading to lung metastases. Mice then received a single IV injection of saline, UTD macrophages (UTD), macrophages transduced with empty Ad5f35 vector (Empty) or anti-HER2 CAR-Ms (Fig. 2a). CAR-treated mice demonstrated a marked reduction in tumor burden (Fig. 2b). Although all mice eventually progressed, a single

infusion of CAR-Ms led to a prolongation of overall survival (Fig. 2c). Given that empty transduced macrophages did not demonstrate anti-tumor activity in vitro or in vivo, in all future experiments we compared UTD with CAR. Co-localization and anti-tumor activity of CAR-M were evaluated by immunohistochemical analysis of explanted lungs, revealing the presence of multiple metastatic tumor nests in this model (Fig. 2d), with a significant reduction in metastatic tumor burden after CAR-M treatment (Fig. 2e).

In the second model, intraperitoneal (IP) carcinomatosis was modeled in NSGS mice via IP injection with SKOV3. Mice were treated 2–4 h later with a single IP injection of saline, UTD macrophages or anti-HER2 CAR-Ms (Fig. 2f). CAR-Ms, but not UTD macrophages, led to marked tumor regression in most treated mice as demonstrated by serial bioluminescent imaging over 100 d (Fig. 2g). The treatment was not associated with significant toxicity as demonstrated by body weights (Supplementary Fig. 2c) and led to significantly improved overall survival in the CAR treatment group (Fig. 2h).

We next sought to evaluate the persistence, biodistribution and trafficking of CAR-M after systemic administration. Using luciferase/CAR co-expressing human macrophages, CAR-M persisted for at least 62 d in vivo in tumor-free NSGS mice (Fig. 2i). To evaluate the ability of human UTD or CAR-M to traffic to established tumor xenografts of multiple types, fluorescently labeled macrophages were administered and the relative signal in the tumor, liver, spleen and lung was evaluated in explanted whole-organ tissue on day 5. Macrophages trafficked to all five solid tumor types that were evaluated (Fig. 2j). Adenoviral transduction did not affect the pattern of macrophage chemokine receptor expression (Supplementary Fig. 2d) and did not affect the trafficking capability of macrophages. In all mice, the liver was the primary normal tissue where macrophages accumulated after IV administration.

Macrophage phenotype is plastic and can change in response to cytokines, pathogen-associated molecular patterns, metabolic cues, cell–cell interactions and tissue-specific signals[28]. Given that adenoviral infection activates the inflammasome, we hypothesized that exposure to Ad5f35, regardless of the encoded transgene, might induce a pro-inflammatory (M1) macrophage phenotype[29,30]. Nonbiased hierarchical clustering of macrophage transcriptomes from four human donors showed that transduced macrophages clustered distinctly from UTD macrophages (Supplementary Fig. 3a). Furthermore, when UTD, Ad5f35-CAR transduced, empty-vector Ad5f35 transduced (Empty), classically activated (M1) and alternatively activated (M2) macrophage transcriptomes from multiple human donors were subjected to nonbiased principal component

Fig. 1 | Generation of human CAR-Ms and assessment of CAR-mediated tumor phagocytosis. a, Assessment of indicated THP-1 macrophage phagocytosis against CD19^{+} K562 target cells using fluorescent microscopy. Data are represented as the mean ± s.e.m. of $n = 3$ technical triplicates, with three random fields of view assessed per replicate. Statistical significance was calculated with one-way ANOVA with multiple comparisons. **b**, Phagocytosis of CD19^{+} or control CD19^{−} K562 target cells by CAR19ζ-expressing THP-1 macrophages. Data are represented as the mean ± s.e.m. of $n = 3$ technical triplicates, with three random fields of view assessed per replicate. Statistical significance was calculated using a two-sided t-test. **c,d**, In vitro phagocytosis by UTD or CAR-meso-ζ THP-1 macrophages of mesothelin+ve K562 cells (**c**) or by CAR-HER2-ζ macrophages of HER2^{+} K562 cells (**d**). Data are represented as mean ± s.e.m. of $n = 3$ technical replicates, with three random fields of view assessed per replicate. Statistical significance was calculated using a two-sided t-test. **e**, Representative FACS plot of CD46 expression on primary human macrophages (blue) or isotype control (red). This graph is representative of $n = 10$ human donors. **f**, Representative FACS plot of CAR-HER2 expression on Ad5f35-transduced primary human macrophages (blue, CAR-M; red, UTD-M). This graph is representative of $n = 10$ human donors. **g**, CAR expression on macrophages derived from $n = 10$ human donors 48 h after Ad5f35-CAR transduction. **h**, Incucyte-based phagocytosis of HER2 functionalized or control pH-Rodo-labeled beads by UTD or CAR-M. Data are represented as mean ± s.e.m. of $n = 3$ technical replicates and are representative of three experiments. Statistical analysis was calculated using a two-sided t-test. **i**, FACS-based phagocytosis of HER2^{−} (MDA-468) or HER2^{+} (SKOV3) target tumor cells by UTD or CAR-M. Statistical significance was calculated with one-way ANOVA with multiple comparisons, and data represent $n = 3$ technical replicates (representative of at least three individual experiments). **j**, Incucyte-based killing assay of GFP[+] SKOV3 by UTD or CAR-M after 48 h of co-culture at different E:T ratios. Statistical significance was calculated with one-way ANOVA with multiple comparisons, and data represent the mean ± s.e.m. of $n = 3$ technical replicates (representative of at least three individual experiments). **k**, Incucyte-based killing kinetics of UTD or CAR-M against SKOV3 at a 10:1 E:T ratio. Data are represented as the mean ± s.e.m. of $n = 3$ technical replicates (representative of at least three individual experiments). For all panels, *$P < 0.05$, **$P < 0.01$, ***$P < 0.001$, ****$P < 0.0001$.

analysis, adenovirally transduced macrophages clustered toward the classically activated and away from the alternatively activated macrophages, regardless of CAR expression (Fig. 3a). Transduction led to the induction of many interferon-associated genes (Fig. 3b), consistent with a classically activated M1 phenotype, and pathway analysis confirmed the induction of M1-associated pathways, such as interferon signaling, pattern recognition receptor signaling, Th1 pathway and iNOS signaling (Supplementary Fig. 3b). Furthermore, key components of the antigen-presentation machinery

such as co-stimulatory ligands, antigen processing and presentation and MHC-Class I/II genes were induced (Supplementary Fig. 3c). We validated the induction of a pro-inflammatory M1 phenotype by quantitative PCR and flow cytometry and demonstrated a dose-dependent response (Supplementary Fig. 3d,e). Induction and repression of these markers were equivalent between CAR and empty vector Ad5f35, demonstrating that the phenotype is induced by the viral vector rather than CAR expression per se in macrophages (Supplementary Fig. 3f). These findings were
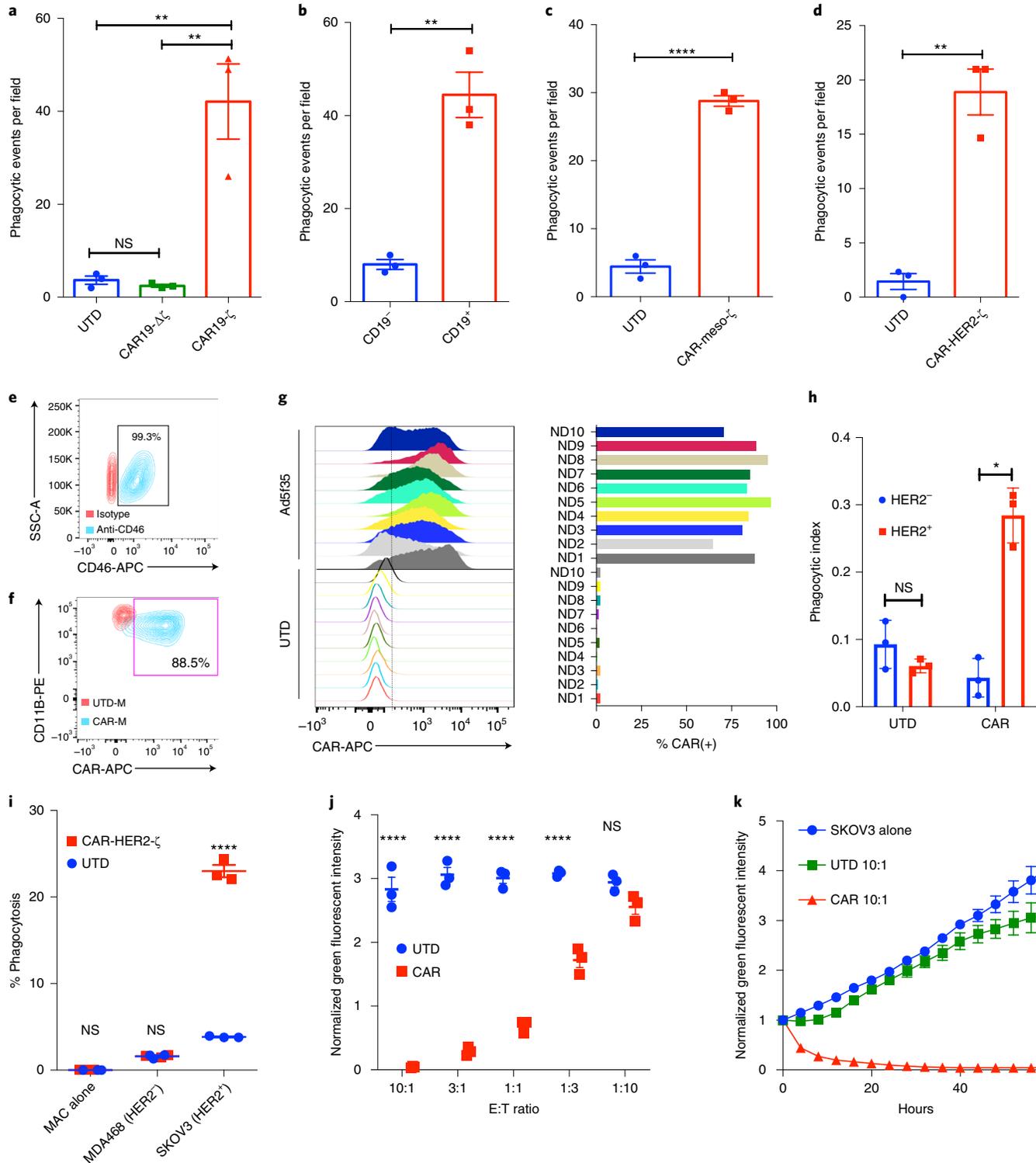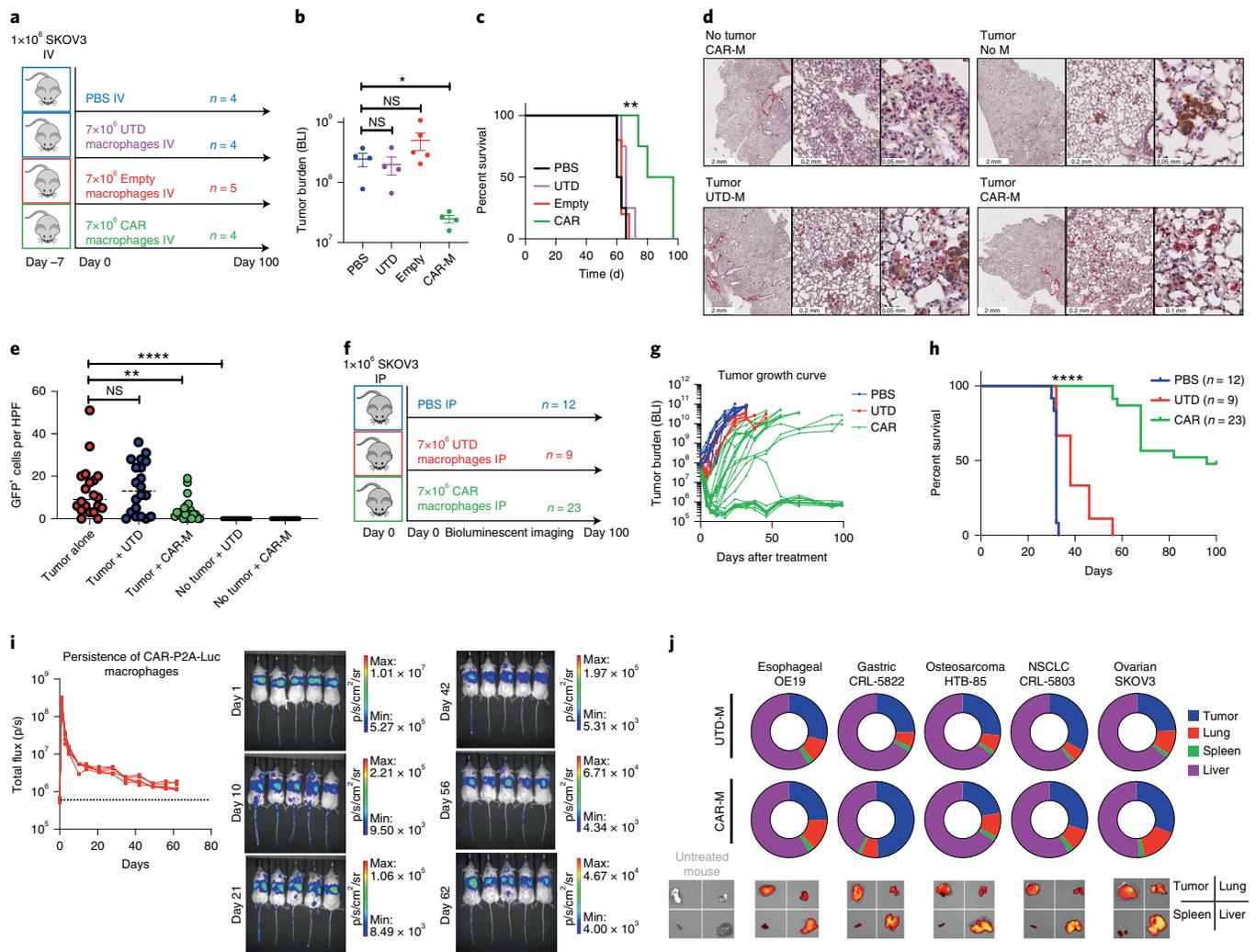
Fig. 2 | Evaluation of anti-tumor activity, persistence and trafficking of primary human anti-HER2 CAR-Ms in xenograft models. a, NSGS mice were IV injected with luciferase(+) SKOV3 and treated with IV PBS, UTD, empty vector transduced (empty) or CAR-HER2 macrophages 7 d later with *n* as shown. **b**, Tumor burden (total flux) by bioluminescent imaging 31 d after treatment. Data are represented as mean ± s.e.m., and statistical significance was calculated with ANOVA with multiple comparisons. **c**, Kaplan–Meier survival curve (median survival, 88.5 d (CAR) versus 63 d (Empty), $P = 0.0047$). Statistical significance was calculated using the log-rank Mantel–Cox test with df = 2. **d**, Lungs from mice with metastatic disease were assessed with dual immunohistochemical analysis (tumor: anti-GFP, brown; macrophage detection: anti-human CD68, red). Each panel shows low (left), medium (middle) and high (right) power view. The experiment was performed once. **e**, Quantification of GFP+ tumor cells in $n = 5$ random ×20 high-power fields per slice, with two slices per mouse and two mice per group. Analysis was done by an observer who was blinded to treatment group allocation. Data are presented as the mean, with statistical significance calculated using multiple two-sided *t*-tests. **f**, NSGS mice were injected with SKOV3 IP 2–4 h before receiving injections of PBS, control (UTD) or CAR-HER2 human macrophages IP as shown. **g**, Tumor burden measured by bioluminescence (total flux) over 100 d. **h**, Kaplan–Meier survival curve over 100 d. Statistical significance was calculated using the log-rank Mantel–Cox test (CAR versus UTD, $P < 0.0001$ with df = 2). **i**, Persistence and biodistribution of CAR-P2A-luciferase-expressing human macrophages after IV administration in $n = 5$ tumor-free NSGS mice. Luciferase signal was tracked over the course of 62 d (dotted line represents background luminescence). Macrophages initially transited through the lung and accumulated in the liver of tumor-free mice. The experiment was performed twice with similar results. **j**, Tumor trafficking and biodistribution of VivoTrack680-labeled UTD or CAR-M in five tumor xenograft models. NSGS mice were killed and organs/tumors were explanted for ex vivo imaging 5 d after a single injection of 5×10^6 UTD or CAR-M, $n = 3$–5 mice per treatment group per tumor type; the experiment was performed once. For all panels, $*P < 0.05, **P < 0.01, ***P < 0.001, ****P < 0.0001$.

validated in macrophages from ten human donors (Supplementary Fig. 3g), and the M1 phenotype was maintained for at least 40 d after transduction (Supplementary Fig. 3h).

Given that CAR-Ms become pro-inflammatory, we sought to evaluate the bidirectional interaction of CAR-Ms with the human TME in a humanized immune system (HIS) mouse model. HIS mice were generated by transplanting female human CD34+ hematopoietic stem cells (HSCs) into NSG mice. After confirmation of human myeloid cells in the peripheral blood, SKOV3 ovarian

tumors were engrafted in the subcutaneous flank and male human UTD or CAR macrophages were injected intratumorally after 19 d. Five days later, tumors were harvested and subjected to single-cell RNA sequencing. The use of female HSCs and male UTD or CAR macrophages allowed the distinction of HSC-derived TME macrophages from adoptively transferred macrophages (Fig. 3c). UTD and CAR macrophages (confirmed by scFv mapping) from within the TME were phenotypically distinct. Although both UTD and CAR macrophages expressed the macrophage identity marker CD68, only

UTD expressed the M2 marker MRC1 (CD206), and only CAR-Ms expressed M1-associated interferon response genes (IFIT1, ISG15 and IFITM1) (Fig. 3d). These data demonstrate that CAR-Ms maintained a pro-inflammatory phenotype within the human TME.

We validated phenotypic plasticity by challenging control or Ad5f35-transduced human macrophages with M2-inducing factors in vitro. Upon stimulation with IL4, IL13 or SKOV3 conditioned media, only UTD macrophages upregulated the canonical M2 marker CD206 (Supplementary Fig. 4a). Furthermore, upon stimulation with IL4, only UTD macrophages increased their basal oxygen consumption rate, an expected characteristic of IL4-induced M2 macrophages (Supplementary Fig. 4b)[31]. Transcriptome analysis revealed that significantly fewer genes were induced by IL4 or IL13 in CAR versus UTD macrophages (Supplementary Fig. 4c,d), including the CD206-encoding M2-associated gene MRC1 (Supplementary Fig. 4e,f).

Using the humanized TME mouse model, the effect of CAR-Ms on the surrounding TME was interrogated at single-cell resolution. Adoptively transferred macrophages were removed from analysis by excluding all human male cells. The human TME grouped into two large clusters (cluster 0 and cluster 1) and one small cluster of cells that was excluded from analysis (cluster 2). Cluster 0 was enriched in the CAR-M-treated arm (86% CAR, 14% UTD), whereas cluster 1 was enriched in the UTD-treated arm (71% UTD, 29% CAR) (Fig. 3e). Gene expression analysis of cluster 0 revealed an enrichment of pro-inflammatory genes such as MHC-II and TNF, demonstrating that CAR-Ms remodeled the TME toward a pro-inflammatory state (Fig. 3f).

To validate these in vivo findings, we evaluated the effect of CAR-Ms on M2 macrophages in vitro and found that CAR-M conditioned media induced a phenotypic shift in M2A, M2C and M2D macrophages (Supplementary Fig. 5a). CAR-Ms induced pro-inflammatory pathways such as interferon signaling, TH1 pathway and iNOS signaling in M2 macrophages (Fig. 3g). Pro-inflammatory marker induction in all M2 macrophage subtypes that were exposed to CAR-Ms was confirmed by FACS (Supplementary Fig. 5b). Additionally, CAR-Ms induced activation and maturation markers in immature human dendritic cells (Fig. 3h) and directly

induced the recruitment of both resting and activated human T cells in an in vitro chemotaxis assay (Fig. 3i). Finally, having shown that CAR-Ms can exert a dominant effect on surrounding immune cells, we demonstrated that CAR-Ms maintained their anti-tumor activity in the presence of human M2 macrophages (Fig. 3j).

Given the upregulation of co-stimulatory ligands and antigen processing and presentation genes and the established role of macrophages as professional antigen-presenting cells (APCs), we sought to test the capacity for CAR-Ms to co-stimulate and present antigens to T cells. To evaluate whether Ad5f35 activation affects the ability of human macrophages to activate T cells, macrophages transduced with the tumor-associated antigen NY-ESO1 and with HLA-A2*01 (Supplementary Fig. 5c,d) were then transduced with Ad5f35, or not (UTD), and co-cultured with autologous antigen-specific T cells (made by transducing CD8+ T cells with clone 1G4 anti-NYESO1 TCR construct[32]). Ad5f35-transduced NY-ESO1-expressing macrophages induced significantly more proliferation of 1G4 CD8+ T cells than NY-ESO1-expressing control macrophages or Ad5f35-transduced macrophages lacking NY-ESO1 (Supplementary Fig. 5e).

To test CAR-M cross-presentation of intracellular tumor antigens ingested during phagocytosis of whole tumor cells, we generated SKOV3 expressing NY-ESO-1 only (SKOV-NY), SKOV3 expressing HLA-A201 and NY-ESO-1 (SKOV-A201-NY) and CAR-Ms from an HLA-A201+ donor. TRAC knockout anti-NYESO1 TCR T cells were incubated with CAR-Ms (macrophage control), SKOV-NY (tumor control), SKOV-A2-NY (positive control) or CAR-Ms that were fed SKOV-NY for 48 h. CD8+ anti-NYESO1 T cells were activated (as determined by CD69 induction and production of IFNγ) by CAR-Ms that ingested SKOV-NY (Fig. 3k). Anti-NYESO1 T cells were not activated by SKOV-NY or CAR-Ms alone, demonstrating that macrophages were able to cross-present tumor-derived antigens after phagocytosis, suggesting that CAR-Ms might lead to epitope spreading.

To test the potential of CAR-Ms to stimulate T cells in vivo, NSGS mice were engrafted with metastatic SKOV3 and treated with CAR-Ms, CAR-Ms plus donor-derived polyclonal T cells or T cells alone. Mice that received CAR-Ms and donor-derived T cells had deeper anti-tumor responses than those that received

Fig. 3 | Adenovirally transduced CAR-Ms are M1 polarized, modify the TME and cross-present tumor antigens. a, Gene expression principal component analysis clustering from UTD, Ad5f35-empty-vector transduced, Ad5f35-CAR-HER2-ζ transduced, classically activated M1 or alternatively activated M2 human macrophages. *n* = 3–4 human donors. **b**, Volcano plot of differentially expressed genes in UTD versus CAR-M. Purple indicates $P_{adj} < 0.05$ and $\log_2$ fold change >1 or <−1. Red triangles indicate significantly upregulated interferon-associated genes (*n* = 4 human donors). Statistical significance was calculated using the Wald test for DESeq2 data. **c**, Schema of HIS TME model generation. Mice were engrafted with human female CD34+ cells, and after human myeloid engraftment was confirmed, SKOV3 tumors were established in the subcutaneous flank. Nineteen days after tumor administration, 1×10^7 UTD or CAR macrophages from a male human donor were injected intratumorally. Tumors were harvested 5 d after treatment, and scRNAseq was performed on the tumor samples. Adoptively transferred macrophages were distinguished from macrophages in the TME by Y-chromosome gene mapping. **d**, Cluster plots demonstrating the phenotypic distinction of UTD from CAR macrophages within the TME (left). On the right, the relative expression of the indicated genes was mapped onto CAR-M (top cluster) or UTD (bottom cluster). The data represent three mice and two mice for the CAR-M and UTD arms, respectively. **e**, Cluster plots demonstrating the phenotypic distinction of human TME after UTD versus CAR-M treatment. Cluster 0 was enriched in the CAR-M-treated arm (86% events from the CAR cohort), whereas cluster 1 was enriched in events from the UTD-treated arm (71% events from the UTD cohort). Cluster 2 was mixed and had few events. **f**, Gene expression heat map from each TME scRNAseq cluster from **e**. Pro-inflammatory genes were found in cluster 0 (annotated in red). Potential anti-inflammatory or M2-associated genes in cluster 1 are annotated in blue. For panels **c**–**f**, *n* = 3 mice per group; the experiment was performed once. **g**, Ingenuity pathway analysis of the transcriptome of in vitro-polarized M2A macrophages after exposure to conditioned media from UTD or CAR-M for 48 h; *n* = 3 technical replicates. Statistical significance was calculated using Fisher's exact test. **h**, Human immature dendritic cells were treated with UTD or CAR-M conditioned media for 48 h, and activation markers CD86 and MHC-II (HLA-DR) were assessed by FACS. Data are represented as the mean ± s.e.m. from *n* = 3 technical replicates. Statistical significance was calculated using a two-tailed *t*-test. **i**, Chemotaxis of resting or activated CD3+ T cells by UTD or CAR-M conditioned media. Data represent T cells from *n* = 4 human donors, and statistical significance was calculated using a paired *t*-test. **j**, Incucyte-based killing assay of SKOV3 by CAR-M alone or in the presence of M0, M2a or M2c macrophages at an E:T:M2 ratio of 3:1:1. Data are represented as the mean ± s.e.m. of *n* = 3 technical replicates. **k**, CAR-M cross-presentation assay showing CD69 induction (left) and IFNγ secretion (right) by anti-NYESO TCR+ T cells 24 h after co-culture with HLA-A201(+) CAR-M (CAR-M, blue), HLA-A201(−)NYESO(+) SKOV3 (SKOV NY, orange) or HLA-A201(+) CAR-M co-cultured with SKOV NY for 48 h (green). Anti-NYESO T cells exposed to HLA-A201(+)NYESO(+) SKOV3 alone were used as positive control (purple). Data are represented as the mean ± s.e.m. of *n* = 3 technical replicates. Statistical analysis was performed using ANOVA with multiple comparisons. For all panels, *P < 0.05, **P < 0.01, ***P < 0.001, ****P < 0.0001. CM, conditioned media.

either CAR-Ms or T cells alone at a late timepoint (Supplementary Fig. 5f). Given that the T cells were not engineered to specifically recognize SKOV3 antigens in this in vivo model, the synergistic effect between CAR-Ms and T cells was likely due to CAR-M-mediated potentiation of nonspecific (that is, allogeneic) T cell anti-tumor activity. The interaction of CAR-Ms with endogenous T cells will be evaluated in syngeneic immunocompetent murine tumor models in future studies.

There is increasing interest in depleting or re-polarizing TAMs to generate an anti-tumor pro-inflammatory effect. However, it is likely that this approach would be successful only if removal of an inhibitory cell type (TAM) were complemented by the addition of

a positive stimulus. We hypothesized that human peripheral blood monocytes could be differentiated to macrophages, endowed with tumor antigen-specific domains and allowed to traffic into tumors. To test this hypothesis, we developed an efficient and robust gene transfer method that had the added benefit of conferring on the engineered macrophages a robust pro-inflammatory signature with the potential to further polarize the surrounding microenvironment. In addition to direct anti-tumor activity by CAR-Ms, we found evidence for cross-presentation and for T cell co-stimulation, thereby raising the possibility that CAR-Ms could directly diminish tumor burden, sculpt the TME and generate a vaccinal effect. Having established a CAR-M platform, in future work we will study
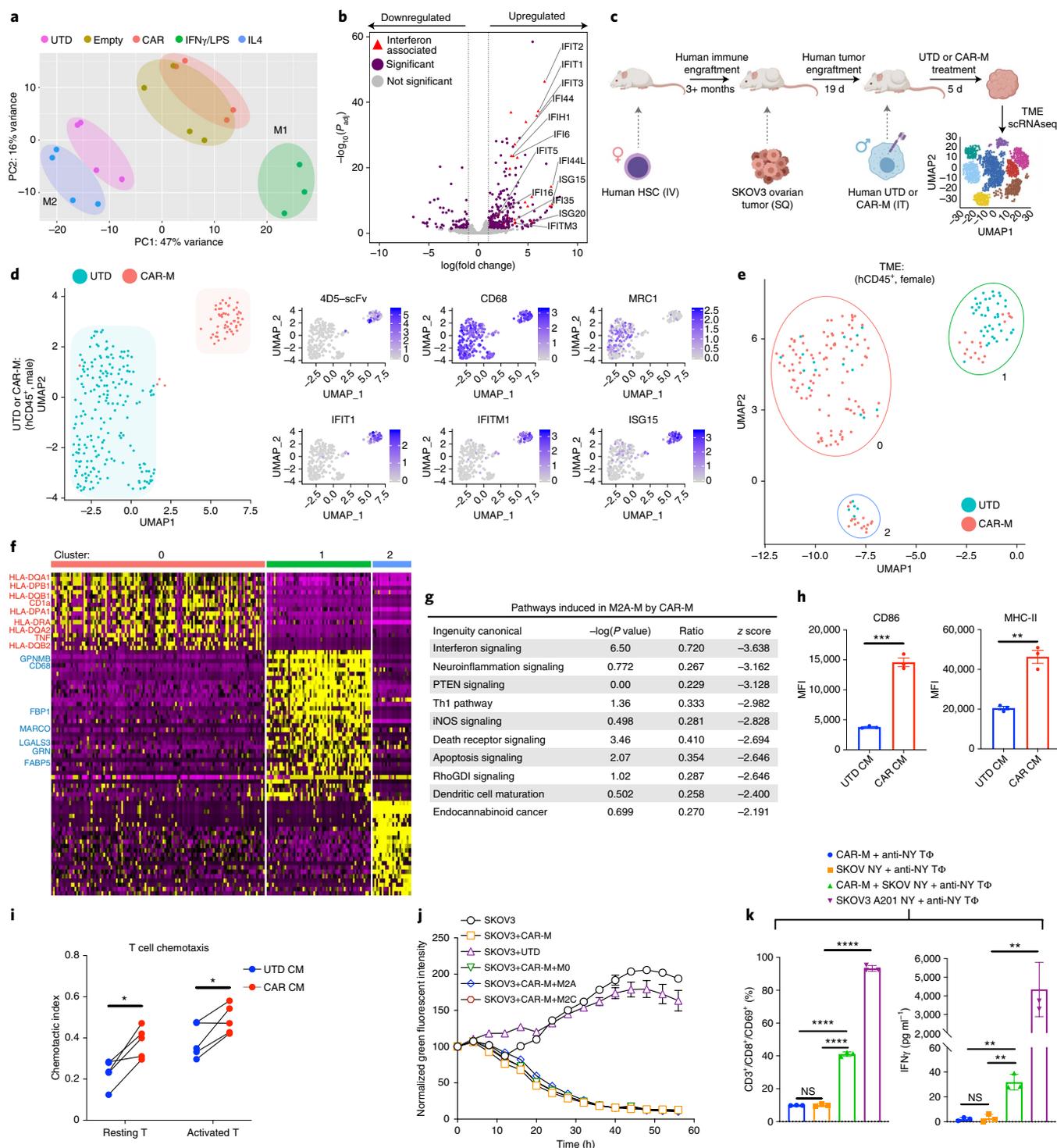
the potential mechanisms of tumor progression and evaluate rational combinations with agents that affect cell death pathways, phagocytosis or T cell-based immunity.

Online content

Any methods, additional references, Nature Research reporting summaries, source data, extended data, supplementary information, acknowledgements, peer review information; details of author contributions and competing interests; and statements of data and code availability are available at https://doi.org/10.1038/s41587-020-0462-y.

References

1. Maude, S. L. et al. Tisagenlecleucel in children and young adults with B-cell lymphoblastic leukemia. *N. Engl. J. Med.* **378**, 439–448 (2018).
2. Schuster, S. J. et al. Chimeric antigen receptor T cells in refractory B-cell lymphomas. *N. Engl. J. Med.* **377**, 2545–2554 (2017).
3. Beatty, G. L. & O'Hara, M. Chimeric antigen receptor-modified T cells for the treatment of solid tumors: defining the challenges and next steps. *Pharmacol. Ther.* **166**, 30–39 (2016).
4. Kingwell, K. CAR T therapies drive into new terrain. *Nat. Rev. Drug Discov.* **16**, 301–304 (2017).
5. Ritchie, D. et al. In vivo tracking of macrophage activated killer cells to sites of metastatic ovarian carcinoma. *Cancer Immunol. Immunother.* **56**, 155–163 (2007).
6. Biswas, S. K., Allavena, P. & Mantovani, A. Tumor-associated macrophages: functional diversity, clinical significance, and open questions. *Semin. Immunopathol.* **35**, 585–600 (2013).
7. Zhang, Q. et al. Prognostic significance of tumor-associated macrophages in solid tumor: a meta-analysis of the literature. *PLoS One* **7**, e50946 (2012).
8. Medrek, C., Pontén, F., Jirström, K. & Leandersson, K. The presence of tumor associated macrophages in tumor stroma as a prognostic marker for breast cancer patients. *BMC Cancer* **12**, 306 (2012).
9. Noy, R. & Pollard, J. W. Tumor-associated macrophages: from mechanisms to therapy. *Immunity* **41**, 49–61 (2014).
10. Lee, H.-W., Choi, H.-J., Ha, S.-J., Lee, K.-T. & Kwon, Y.-G. Recruitment of monocytes/macrophages in different tumor microenvironments. *Biochim. Biophys. Acta* **1835**, 170–179 (2013).
11. Mantovani, A., Marchesi, F., Malesci, A., Laghi, L. & Allavena, P. Tumour-associated macrophages as treatment targets in oncology. *Nat. Rev. Clin. Oncol.* **14**, 399–416 (2017).
12. Morrison, C. Immuno-oncologists eye up macrophage targets. *Nat. Rev. Drug Discov.* **15**, 373–374 (2016).
13. Weiskopf, K. Cancer immunotherapy targeting the CD47/SIRPα axis. *Eur. J. Cancer* **76**, 100–109 (2017).
14. Weiskopf, K. & Weissman, I. L. Macrophages are critical effectors of antibodies therapies for cancer. *MAbs* **7**, 303–310 (2015).
15. Weiskopf, K. et al. Engineered SIRPα variants as immunotherapeutic adjuvants to anticancer antibodies. *Science* **341**, 88–91 (2013).
16. Roghanian, A., Stopforth, R. J., Dahal, L. N. & Cragg, M. S. New revelations from an old receptor: immunoregulatory functions of the inhibitory Fc gamma receptor, FcγRIIB (CD32B). *J. Leukoc. Biol.* **103**, 1077–1088 (2018).
17. Franken, L., Schiwon, M. & Kurts, C. Macrophages: sentinels and regulators of the immune system. *Cell. Microbiol.* **18**, 475–487 (2016).
18. Barrio, M. M. et al. Human macrophages and dendritic cells can equally present MART-1 Antigen to CD8+ T cells after phagocytosis of gamma-irradiated melanoma cells. *PLoS One* **7**, e40311 (2012).
19. Tang-Huau, T.-L. et al. Human in vivo-generated monocyte-derived dendritic cells and macrophages cross-present antigens through a vacuolar pathway. *Nat. Commun.* **9**, 2570 (2018).
20. Hume, D. A. Macrophages as APC and the dendritic cell myth. *J. Immunol.* **181**, 5829–5835 (2008).
21. Andreesen, R., Hennemann, B. & Krause, S. W. Adoptive immunotherapy of cancer using monocyte-derived macrophages: rationale, current status, and perspectives. *J. Leukoc. Biol.* **64**, 419–426 (1998).
22. Thiounn, N. et al. Adoptive immunotherapy for superficial bladder cancer with autologous macrophage activated killer cells. *J. Urol.* **168**, 2373–2376 (2002).
23. Burger, M. et al. The application of adjuvant autologous antravesical macrophage cell therapy vs. BCG in non-muscle invasive bladder cancer: a multicenter, randomized trial. *J. Transl. Med.* **8**, 54 (2010).
24. Gaggar, A., Shayakhmetov, D. M. & Lieber, A. CD46 is a cellular receptor for group B adenoviruses. *Nat. Med.* **9**, 1408–1412 (2003).
25. Nilsson, M. et al. Development of an adenoviral vector system with adenovirus serotype 35 tropism; efficient transient gene transfer into primary malignant hematopoietic cells. *J. Gene Med.* **6**, 631–641 (2004).
26. Fleetwood, A. J., Lawrence, T., Hamilton, J. A. & Cook, A. D. Granulocyte-macrophage colony-stimulating factor (CSF) and macrophage CSF-dependent macrophage phenotypes display differences in cytokine profiles and transcription factor activities: implications for CSF blockade in inflammation. *J. Immunol.* **178**, 5245–5252 (2007).
27. Wunderlich, M. et al. AML xenograft efficiency is significantly improved in NOD/SCID-IL2RG mice constitutively expressing human SCF, GM-CSF and IL-3. *Leukemia* **24**, 1785–1788 (2010).
28. Mosser, D. M. & Edwards, J. P. Exploring the full spectrum of macrophage activation. *Nat. Rev. Immunol.* **8**, 958–969 (2008).
29. Lam, E., Stein, S. & Falck-Pedersen, E. Adenovirus detection by the cGAS/STING/TBK1 DNA sensing cascade. *J. Virol.* **88**, 974–981 (2014).
30. Muruve, D. A. et al. The inflammasome recognizes cytosolic microbial and host DNA and triggers an innate immune response. *Nature* **452**, 103–107 (2008).
31. Kelly, B. & O'Neill, L. A. Metabolic reprogramming in macrophages and dendritic cells in innate immunity. *Cell Res.* **25**, 771–784 (2015).
32. Robbins, P. F. et al. A pilot trial using lymphocytes genetically engineered with an NY-ESO-1-reactive T-cell receptor: long-term follow-up and correlates with response. *Clin. Cancer Res.* **21**, 1019–1027 (2015).

Methods

Cell lines. The THP-1, SKOV3, K562, MDA-468, CRL-2351, HTB-20, HTB-85, CRL-5803, CRL-5822, CRL-1555, HTB-131, HTB-20 and CRL-1902 cell lines were purchased from the American Type Culture Collection (ATCC). Cells were cultured in RPMI media with 10% FBS, penicillin, streptomycin, 1× GlutaMAX and 1× HEPES unless otherwise recommended by the ATCC. All cell lines were transduced with a lentiviral vector co-encoding click beetle green (CBG) luciferase and green florescent protein (GFP) under an EF1α promoter, separated by a P2A sequence. Transduced target cell lines were FACS sorted for 100% GFP positivity before use as targets in vitro and in vivo. THP-1 cells were lentivirally transduced, FACS sorted and maintained in liquid culture. CAR expression and purity were routinely validated.

Plasmid construction and virus. For lentivirus production, CAR constructs were cloned into the third-generation pTRPE lentiviral backbone using standard molecular biology techniques. All CAR constructs used a CD8 leader sequence, (GGGGS)₃ linker, CD8 hinge and CD8 transmembrane domain and were expressed under the control of an EF1α promoter. Lentivirus was packaged in HEK293 cells and purified and concentrated as described previously[33]. In indicated experiments, Vpx was incorporated into lentivirus at the packaging stage as previously described[34]. Cell lines were transduced with lentivirus MOI 3–5 unless otherwise noted. For replication-deficient adenovirus production, anti-HER2 CAR was cloned into the pShuttle transfer plasmid using *Xba-I* and *Sal-I* and subsequently cloned into pAd5f35 using *I-Ceu I* and *PI-Sce I*. All cloning steps were validated by restriction enzyme digest and sequencing. pAd5f35 is first-generation E1/E3 deleted adenoviral backbone. Ad5f35-CAR-HER2-ζ was generated, expanded, concentrated and purified using standard techniques in 293 cells by the Baylor Vector Development Laboratory. All adenoviral batches were verified negative for replication-competent adenovirus and passed sterility and endotoxin analysis. Adenoviral titer was determined using Adeno-X Rapid Titer Kit (Clontech) and validated by functional transgene expression in human macrophages. An MOI of 1,000 plaque-forming units (PFU) per cell was used unless otherwise stated.

Animal studies. All mouse studies were conducted in accordance with national guidelines for the humane treatment of animals and were approved by the Institutional Animal Care and Use Committee (IACUC) at the University of Pennsylvania. Schemas of the used xenograft models are shown in detail in the first panel of each relevant figure. NOD/SCID *Il2rg*⁻/⁻ hIL3-hGMCSF-hSF (NSG-SM3 or NSGS) mice originally obtained from Jackson Laboratories were purchased and bred by the Stem Cell and Xenograft Core at the University of Pennsylvania. Cells (SKOV3 tumor cells, human macrophages or human T cells) were injected in 200–300 ul PBS for both IP and IV tail vein injections. IV injections of human macrophages were split into consecutive injections to attain the target dose. Bioluminescent imaging was performed at least weekly using an IVIS Spectrum (PerkinElmer) and analysis was performed using LivingImage v4.3.1 (Caliper Life Sciences). Mice were weighed weekly and were subject to routine veterinary assessment for signs of overt illness. Animals were killed at experimental termination or when predetermined IACUC rodent health endpoints were reached.

Flow cytometry. Primary human macrophages were tested for CAR-HER2 expression using a two-step staining protocol: human HER2/ERBB2 Protein-His tag (10004-H08H-100, Sino Biological) primary stain followed by Human TruStain FcX (422302, BioLegend) and Anti-His Tag APC (IC050A, R&D Systems) secondary stain. TruStain FcX (422302, BioLegend) was always used for FACS staining of monocytes, macrophages or monocytic cell lines expressing Fc receptors. Macrophage purity was tested using the following panel: Anti-CD11b PE (301306, BioLegend), Anti-CD14 BV711 (301838, BioLegend), Anti-CD3 FITC (11-0038-42, eBioscience), Anti-CD19 PE-CY7 (25-0198-42, eBioscience), Anti-CD66b PerCP-CY5.5 (305108, BioLegend), Anti-CD56 BV605 (318334, BioLegend) and Live/Dead Fixable Aqua (L/D Aqua) Dead Cell Stain Kit (L34957, Thermo Fisher). The same panel was used for testing the monocyte purity after CD14 MACS selection, before seeding for differentiation. M1 and M2 markers on primary human macrophages were detected with the following panel: Anti-CD11B PE (301306, BioLegend), Anti-CD80 BV605 (305225, BioLegend), Anti-CD86 BV711 (305440, BioLegend), Anti-CD206 BV421 (321126, BioLegend), Anti CD163 APC-CY7 (333622, BioLegend), Anti-HLA-DR BV785 (307642, BioLegend), Anti-HLA ABC PE/CY7 (311430, BioLegend) and Live/Dead Fixable Aqua Dead Cell Stain Kit. CD46 expression was detected with Anti-CD46 APC (352405, BioLegend) and CXADR was detected with Anti-CAR PE (FCMAB418PE-I, EMD Millipore). Appropriate fluorescence-matched isotype controls were acquired from BioLegend. Surface HER2 was detected using Anti-Human CD340/HER2 APC (324408, BioLegend). Flow cytometry data were acquired on a BD Fortessa with HTS (BD Biosciences) and analyzed with FlowJo X10 (FlowJo).

FACS-based phagocytosis assay. Next, 1×10^5 UTD or CAR-HER2-ζ human monocyte-derived macrophages (48 h after transduction) were co-cultured with media (MAC alone), 1×10^5 GFP⁺ MDA-468 cells (HER2⁻) or 1×10^5 GFP⁺ SKOV3 (HER2⁺) target cells for 3–4 h at 37 °C in triplicate. After co-culture, cells were harvested with Accutase (Innovative Cell Technologies), stained with

Anti-CD11b APC-CY7 (301342, BioLegend) and analyzed with FACS using a BD Fortessa (Becton Dickinson). The percent of GFP⁺ events within the CD11b⁺ population was plotted as percentage phagocytosis. Data are represented as mean ± standard error of triplicate wells. Statistical significance between CAR-HER2-ζ and UTD was calculated using ANOVA with multiple comparisons; ****$P < 0.0001$; NS, nonsignificant.

Bead-based phagocytosis assay. Strepavidin-coated polystyrene microparticles (5.0–5.9-μm diameter, Spherotech) were sterilized for 20 min in 70% isopropanol. Beads were spun down and resuspended in 0.1 M sodium bicarbonate buffer (pH 8.5) and labeled with 10 μM pHrodo SE (Thermo Fisher) for 30 min in the dark. Beads were spun down to remove free dye and resuspended in 0.1 PB (pH 6.5). Biotinylated proteins from ACROBiosystems were added to the beads at a concentration sufficient to occupy one quarter of the binding sites. Beads were incubated with protein for 1 h, washed and resuspended in PBS for use in experiments.

UTD or CAR macrophages were thawed and plated at a density of 2×10^4 viable cells per well in a 96-well plate and allowed to adhere overnight. The next day, the media was aspirated and previously functionalized or blank beads in TexMACS and 10% FBS were added to obtain a 5:1 bead-to-cell ratio. Changes in fluorescence were monitored with IncuCyte Live-Cell Analysis System (Essen BioScience). The phagocytic index was calculated by subtracting the red image mean of wells containing only beads from that of wells with cells and beads and then dividing by the red image mean of the bead-only wells.

Primary cells. Normal donor apheresis was either performed at the hematology unit at the Hospital of the University of Pennsylvania under an institutional review board-approved protocol through the Human Immunology Core of the University of Pennsylvania or acquired and shipped fresh from HemaCare. Apheresis-derived leukopacs were subjected to elutriation using an Elutra Cell Separation System (Terumo BCT) to reduce erythrocytes, platelets, lymphocytes and granulocytes. Monocyte-enriched fractions were pooled and subjected to MACS CD14-positive selection (Miltenyi Biotec) according to the manufacturer's instructions. The pre-selection and post-selection (positive and negative fraction) purity was tested using flow cytometry. Selected CD14 monocytes were seeded in Cell Differentiation Bags (Miltenyi Biotec) in RPMI with 10% FBS, penicillin, streptomycin, 1× GlutaMAX, 1× HEPES and 10 ng ml⁻¹ recombinant human GM-CSF (300-03, PeproTech) for 7 d. Differentiation was monitored by light microscopy. Adenovirus was added on day 5 at an MOI of 1×10^3 based on PFU titer. Differentiated macrophages were harvested at day 7 and tested for CAR expression, differentiation and macrophage purity by FACS. For smaller-scale experiments, macrophages were plated directly in tissue-culture-treated well plates or flasks and transduced at an MOI of 1,000 PFU directly in well plates or flasks. CD3-selected T cells were provided by the University of Pennsylvania Human Immunology Core and were expanded and transduced as previously described[33]. Immature dendritic cells were generated from CD14⁺ monocytes using GM-CSF (100 ng ml⁻¹) and IL-4 (20 ng ml⁻¹) for 9 d.

Microscopy. *Microscopy-based phagocytosis assay.* Control or CAR-expressing monomeric red fluorescent protein-positive (mRFP⁺) THP1 cells were plated at 7.5×10^4 per well in 48-well plates and differentiated with 1 ng ml⁻¹ phorbol 12-myristate 13-acetate (PMA) in RPMI with 10% FBS for 48 h. After differentiation, PMA was washed out with media and 7.5×10^4 control or target GFP⁺ K562 tumor cells were added and co-cultured for 4 h at 37 °C. After 4 h, tumor cells (nonadherent) were washed out and the plate was imaged for mRFP and GFP fluorescence. The average number of phagocytic events in three random fields of view per well were averaged, in triplicate wells, on a ×10 field of view. Cells were imaged using an EVOS FL Auto 2 Imaging System (AMAFD2000, Thermo Fisher). Data represent the mean ± standard error of triplicate wells. Statistical significance was calculated using a *t*-test.

Live video imaging microscopy. Next, 3.0×10^5 CAR or control mRFP⁺ THP-1 cells were differentiated as above in six-well plates and co-cultured with 3.0×10^5 control or target GFP⁺ K562 cells for 16–24 h in an incubated 37 °C live imaging chamber and imaged every 30–120 s for mRFP and GFP using the EVOS FL Auto 2 Live Imaging System (Thermo Fisher) using the ×10 lens.

In vitro cytotoxicity assay. CBG/GFP double-positive SKOV3, HTB-20 and CRL-2351 tumor cells were used as targets in luciferase-based killing assays by control (UTD) or CAR-HER2-ζ (CAR) macrophages. The effector-to-target (E:T) ratio was serially titrated from 10:1 down to 1:30 for both effector groups. Bioluminescence was measured using an IVIS Spectrum (PerkinElmer). Percent specific lysis was calculated on the basis of luciferase signal (total flux) relative to tumor alone, using the following formula.

$$\% \text{ Specific Lysis} = [(\text{Sample signal} - \text{Tumor alone signal})/(\text{Background signal} - \text{Tumor alone signal})] \times 100$$

Data are shown as mean ± s.e.m., with each condition in triplicate. Negative specific lysis values indicate more signal than in the tumor-alone wells. Statistical significance was calculated using ANOVA with multiple comparisons; ****$P < 0.0001$, ***$P < 0.001$, **$P < 0.01$, *$P < 0.05$; NS, nonsignificant.

Image cytometry. Control or CAR mRFP+ THP-1s were differentiated and co-cultured with CD19+GFP+ K562 target cells as described above. After 4 h of co-culture, cells were washed and harvested with trypsin-EDTA and stained with L/D Aqua for viability. Imaging cytometry was performed on Amnis ImageStreamX (EMD Millipore). Cells were gated for mRFP+GFP+ double-positive events and the phagocytosis-identification algorithm (Amnis ImageStreamX) was applied, which identifies GFP signal within an mRFP+ event.

Macrophage polarization. For M1 or classically activated macrophage polarization, human monocyte-derived macrophages were exposed to 20 ng ml^{-1} recombinant interferon-γ (300–02, PeproTech) and 100 ng ml^{-1} lipopolysaccharide (tlrl-eklps, InvivoGen) in RPMI with 10% FBS for 24 h. Where described, human monocyte-derived macrophages were exposed to 20 ng ml^{-1} recombinant human IL4 (200-04, PeproTech) or IL13 (200-13, PeproTech). In some experiments, 48-h conditioned media from SKOV3 was used (50% diluted in RPMI with 10% FBS) to polarize macrophages toward M2 for 24 h. In experiments where control or CAR macrophages were challenged with M2-inducing cytokines, cells were treated with cytokine for 24 h, 48 h after viral transduction. To generate different subtypes of M2 macrophages, the below protocols were used. All human cytokines were purchased from PeproTech.

M2A: 100 ng ml^{-1} M-CSF (7 d); 20 ng ml^{-1} IL-13 and 20 ng ml^{-1} IL-4 (2 d)
M2C: 100 ng ml^{-1} M-CSF (7 d); 10 ng ml^{-1} IL-10 and 10 ng ml^{-1} TGF-β1 (2 d)
M2D: 100 ng ml^{-1} M-CSF (7 d); 50 ng ml^{-1} IL-6; 20 ng ml^{-1} LIF (2 d)

RNA sequencing of human macrophages. RNA was isolated from human macrophages from matched donors, treated as described in each figure and polarized and challenged as above using Ambion RiboPure RNA Purification Kit (AM1924, Thermo Fisher). RNA-seq libraries were generated using TruSeq RNA Library Prep Kit (RS-122-2001/2, Illumina) and validated with BioA by the University of Pennsylvania Next Generation Sequencing Core facility before sequencing. The libraries were sequenced on 75-bp single-end reads using a NextSeq sequencer (Illumina). Low-quality reads were trimmed using Trimmomatic (v0.36) and mapped to human genome (hg38) using STAR (v2.6.0c) with default parameters. Gene count was calculated using featureCounts (v1.6.1)[35]. Nonexpressed genes with read counts <1 in all samples were removed before differential expression analysis. DESeq2 with log fold change of 1 and adjusted P value of 0.05 was used to identify differentially expressed genes.

For genome browser tracks, bam files were first converted into bed files using bedtools (v2.27.1). Normalized bedgraph tracks were generated using makeUCSCfile with 10,000,000 normalization factor (Homer v2) and converted into bigwig format for integrative genomics viewer (IGV; Broad Institute) usage. Reads were mapped to the human genome (hg38) using RUM before using DegSeq and EdgeR for differential analysis. Group auto-scale was applied to all conditions for y-axis equalization in IGV. Ingenuity Pathway Analysis (Qiagen) was used to map differentially expressed genes to canonical pathways.

Real-time PCR. RNA was isolated using Ambion RiboPure RNA Purification Kit (AM1924, Thermo Fisher) and reverse transcribed using iScript RT Supermix for RT-qPCR (1708841, Bio-Rad). For quantitative PCR, template cDNA, primers, Taqman Gene Expression primer/probe and Taqman Gene Expression Master Mix (4369016, Applied Biosystems) were used according to the manufacturer's instructions. The following human primer/probes from Applied Biosystems were used: TNF (Hs00174128_m1), IL12A (Hs01073447_m1), GAPDH (Hs02786624_G1), TAP1 (Hs00388675_m1), CD206 (Hs00267207_m1), CD80 (Hs01045161_m1) and IFNβ (Hs01077958_s1).

T cell stimulation assays. *NY-ESO-1 antigen processing and presentation assay.* Primary human macrophages were transduced with HLA-A201-P2A-NY-ESO1 Vpx lentivirus or not (Ag and No Ag, respectively). 1G4 NY-ESO-1 TCR T cells were generated as previously described and stained with CellTrace Violet (CTV) Cell Proliferation Kit (C34557, Thermo Fisher) according to the manufacturer's instructions[36]. Forty-eight hours after lentiviral transduction, macrophages were transduced with Ad5f35-CAR-HER2-ζ for polarization, or not, for an additional 48 h before the addition of CTV-labeled 1G4 anti-NY-ESO1 TCR autologous T cells for 5 d. Proliferation of anti-NYESO1 TCR+CD8+ T cells was determined by FACS by measuring dilution of CTV.

NY-ESO-1 cross-presentation assay. CAR-Ms were generated from an HLA-A0201+ normal donor leukopack. SKOV3 was transduced with lentiviral vectors to express NY-ESO-1 only or HLA-A0201 and NY-ESO-1. NY-ESO-1-specific T cells were generated by transducing human T cells with a lentivirus encoding the 1G4 anti-NYESO-1 specific TCR and knocking out TRAC using CRISPR–Cas9 to reduce background activation, as previously described[37]. Next, 5×10⁴ CAR-Ms were cultured with 1×10⁴ SKOV-NY or SKOV-A0201-NY for 48 h in 96-well plates. As controls, macrophages and SKOV variants were also cultured separately. Then, 1×10⁵ T cells were added to each condition. Twenty-four and 96 h later, T cells were analyzed for activation markers using FACS. The following antibodies were used: human CD4 PerCP/Cy5.5 (344608, BioLegend), human CD8 BV421 (344748, BioLegend), human CD3 BV711 (317328, BioLegend), human CD11b

FITC (101206, BioLegend), human CD69 PE (3110906, BioLegend) and L/D Aqua (Thermo Fisher). Additionally, T cell activation was evaluated by measurement of IFNγ in the supernatant using MSD U-Plex Kits (Meso Scale Diagnostics).

Mitochondrial respiratory analysis in human macrophages. Mitochondrial function was assessed using an extracellular flux analyzer (Agilent Seahorse Bioscience). Primary human control or CAR macrophages (48 h after transduction), with or without 24-h exposure to 20 ng ml^{-1} recombinant human IL-4 (200-04, PeproTech) were seeded at 1×10⁵ cells per well onto XF96 cell culture microplates. To assay mitochondrial function, the medium was replaced with XF assay base medium supplemented with 5.5 mM glucose, 2 mM L-glutamine and 1 mM sodium pyruvate. Before use, XF96 assay cartridges were calibrated in accordance with the manufacturer's instructions. During instrument calibration (60 min) the cells were switched to a CO_2-free, 37 °C incubator. Cellular oxygen consumption rates and extracellular acidification levels were measured under basal conditions and after treatment with 1.5 µM oligomycin, 1.5 µM fluoro-carbonyl cyanide phenylhydrazone and 40 nM rotenone, with 1 µM antimycin A.

Single-cell RNA-seq. Raw sequencing reads were mapped to the customized human reference genome (GRCH38) using CellRanger V3 (10× Genomics). CellRanger-filtered cells and their gene expression profiles were further processed using Seurat v3.0.1 (https://doi.org/10.1101/460147). For additional quality control, any cells with fewer than 500 expressed genes, with an unusually high number of unique molecular identifier counts (above 3 median absolute deviations) or with high mitochondrial RNA expression (above 3 median absolute deviations) were removed. To compare T cells between UTD and CAR macrophage samples, libraries from UTD and CAR macrophage samples were first merged and corrected for batch effect using the fastMNN package (https://doi.org/10.1038/nbt.4091) from Seurat Wrappers. Next, all cells were clustered with 0.4 resolution and visualized using UMAP reduction with reduction = mnn and dims = 1:30 parameters. Then, T cells that were *GFP* negative, *RPS4Y1* negative and positive for *CD3D* and *PTPRC* were isolated and reclustered. Finally, differentially expressed genes among clusters were identified using FindMarkers function with threshold values of min.pct = 0.25 and log fold change = 0.5.

T cell chemotaxis. Human CD3+ cells were separated using CD3 microbeads (Miltenyi Biotec) in a MACS cell separation column (Miltenyi Biotec) according to the manufacturer's instructions. Purity of the retained fraction was more than 95% CD3+, as assessed by flow cytometry. Resting T cells were labeled using CFSE (Thermo Fisher) according to the manufacturer's instructions and used immediately after being resuspended in RPMI and 0.5% BSA. In some cases, T cells were activated before CFSE labeling using CD3/CD28 Dynabeads (Thermo Fisher) along with 30 U ml^{-1} IL-2 (PeproTech) for 72 h.

Next, 96-well transwell systems (Corning) were functionalized with 10 µg ml^{-1} of fibronectin (R&D Systems) in PBS for 3 h at 37 °C. The PBS solution was carefully aspirated, and labeled T cells were added to the top of the inserts. Conditioned media was then added to the bottom of the wells. After 4 h, the insert was removed and the media in the bottom reservoir was read for CFSE using a plate reader. The chemotactic index was defined as the fractional difference in fluorescence between treatment conditions and RPMI control, divided by the fluorescence of the control.

Statistics. Statistical analysis was performed in GraphPad Prism 6.0 (GraphPad). Each figure legend denotes the statistical test used. All central tendencies indicate the mean, and all error bars indicate s.e.m. unless otherwise indicated. ANOVA multiple-comparison P values were generated using Tukey's multiple-comparisons test. All t-tests were two-sided unless otherwise indicated. For all figures, * indicates $P < 0.05$, ** indicates $P < 0.01$, *** indicates $P < 0.001$ and **** indicates $P < 0.0001$.

Reporting Summary. Further information on research design is available in the Nature Research Reporting Summary linked to this article.

Data availability
RNA sequencing data that support the findings of this study will be deposited and made publicly available in the NCBI Gene Expression Omnibus repository under accession numbers GSE120084 and GSE120086.

References
33. Gill, S. et al. Preclinical targeting of human acute myeloid leukemia and myeloablation using chimeric antigen receptor-modified T cells. *Blood* **123**, 2343–2354 (2014).
34. Bobadilla, S., Sunseri, N. & Landau, N. R. Efficient transduction of myeloid cells by an HIV-1-derived lentiviral vector that packages the Vpx accessory protein. *Gene Ther.* **20**, 514–520 (2013).
35. Liao, Y., Smyth, G. K. & Shi, W. featureCounts: an efficient general purpose program for assigning sequence reads to genomic features. *Bioinformatics* **30**, 923–930 (2014).

36. Rapoport, A. P. et al. NY-ESO-1-specific TCR-engineered T cells mediate sustained antigen-specific antitumor effects in myeloma. *Nat. Med.* **21**, 914–921 (2015).
37. Ren, J. et al. Multiplex genome editing to generate universal CAR T cells resistant to PD1 inhibition. *Clin. Cancer Res.* **23**, 2255–2266 (2017).

Acknowledgements

Author contributions

M.K. and S.G. conceived the study. M.K., M.R., S.G. and C.J. designed key experiments and provided conceptual guidance. M.K., O.S., A.B., K.B., M.S.K., S.K., M.Y.K., R.O., D.M., K.G., N.A., Y.O., M.Z., M.S., X.S., K.V., K.C., N.P. and S.W. carried out experiments. B.G. supervised D.M. X.L. and M.S. performed bioinformatics analysis. M.K. and S.G. wrote the manuscript. S.G. and C.J. provided supervision and mentorship, and S.G. provided funding for the study.

Competing interests

Additional information

Supplementary information is available for this paper at https://doi.org/10.1038/s41587-020-0462-y.

Correspondence and requests for materials should be addressed to S.G.

Reprints and permissions information is available at www.nature.com/reprints.

nature research

Corresponding author(s):   Saar Gill

Last updated by author(s): Nov 26, 2019

Reporting Summary

Nature Research wishes to improve the reproducibility of the work that we publish. This form provides structure for consistency and transparency in reporting. For further information on Nature Research policies, see Authors & Referees and the Editorial Policy Checklist.

Statistics

For all statistical analyses, confirm that the following items are present in the figure legend, table legend, main text, or Methods section.

n/a	Confirmed	
☐	☒	The exact sample size (*n*) for each experimental group/condition, given as a discrete number and unit of measurement
☐	☒	A statement on whether measurements were taken from distinct samples or whether the same sample was measured repeatedly
☐	☒	The statistical test(s) used AND whether they are one- or two-sided *Only common tests should be described solely by name; describe more complex techniques in the Methods section.*
☐	☒	A description of all covariates tested
☐	☒	A description of any assumptions or corrections, such as tests of normality and adjustment for multiple comparisons
☐	☒	A full description of the statistical parameters including central tendency (e.g. means) or other basic estimates (e.g. regression coefficient) AND variation (e.g. standard deviation) or associated estimates of uncertainty (e.g. confidence intervals)
☐	☒	For null hypothesis testing, the test statistic (e.g. *F*, *t*, *r*) with confidence intervals, effect sizes, degrees of freedom and *P* value noted *Give P values as exact values whenever suitable.*
☒	☐	For Bayesian analysis, information on the choice of priors and Markov chain Monte Carlo settings
☒	☐	For hierarchical and complex designs, identification of the appropriate level for tests and full reporting of outcomes
☒	☐	Estimates of effect sizes (e.g. Cohen's *d*, Pearson's *r*), indicating how they were calculated

Our web collection on statistics for biologists contains articles on many of the points above.

Software and code

Policy information about availability of computer code

Data collection	LivingImage software v. 4.3.1 (Caliper LifeSciences), FCS Diva (BD), Illumina NextSeq platform, EVOS FL2 Auto (Life Sciences), Incucyte S3 Software (Sartorius), Attune NXT Software Version 3.1 (Thermo Fisher), MSD Discovery Workbench Version 4.0 (Meso Scale Diagnostics)
Data analysis	GraphPad Prism 6.05 (GraphPad Software, Inc.), FlowJo v.10 (FlowJo LLC), Fiji software (ImageJ), LivingImage software v. 4.3.1 (Caliper LifeSciencies), Excel (Microsoft), Trimmomatic (v0.36), STAR (v2.6.0c), featureCounts (v1.6.1), bedtools (v2.27.1), makeUCSCfile, IGV (Broad Institute), RUM, Ingenuity Pathway Analysis (Qiagen Bioinformatics), Incucyte S3 Software (Sartorius), MSD Discovery Workbench Version 4.0 (Meso Scale Diagnostics)

For manuscripts utilizing custom algorithms or software that are central to the research but not yet described in published literature, software must be made available to editors/reviewers. We strongly encourage code deposition in a community repository (e.g. GitHub). See the Nature Research guidelines for submitting code & software for further information.

Data

Policy information about availability of data

All manuscripts must include a data availability statement. This statement should provide the following information, where applicable:

- Accession codes, unique identifiers, or web links for publicly available datasets
- A list of figures that have associated raw data
- A description of any restrictions on data availability

All requests for raw and analyzed data and materials are promptly reviewed by the University of Pennsylvania Center for Innovation to see if the request is subject to any intellectual property or confidentiality obligations. Any data and materials that can be shared will be released via a Material Transfer Agreement. All raw sequencing data can be found at the NCBI Sequence Read Archive (accession number: not yet available, data actively being uploaded).

Field-specific reporting

Please select the one below that is the best fit for your research. If you are not sure, read the appropriate sections before making your selection.

☒ Life sciences   ☐ Behavioural & social sciences   ☐ Ecological, evolutionary & environmental sciences

For a reference copy of the document with all sections, see nature.com/documents/nr-reporting-summary-flat.pdf

Life sciences study design

All studies must disclose on these points even when the disclosure is negative.

Sample size	Sample size was calculated by estimating the confidence interval and margin of error, or experiments were ran in at least duplicate/triplicate.
Data exclusions	No relevant data were excluded. A priori criteria for exclusion were developed.
Replication	All experiments were conducted in duplicate or triplicate. When available and possible we used macrophages derived from multiple normal donors and different cell lines. All attempts at replication were successful.
Randomization	Randomization was not relevant to this work. For in vivo models, baseline tumor burden was verified as equivalent (i.e. there was no statistically significant difference amongst the groups via ANOVA) between treatment groups.
Blinding	Blinding analysis was implented in quantification of tumor cells in immunohistochemistry sections.

Reporting for specific materials, systems and methods

We require information from authors about some types of materials, experimental systems and methods used in many studies. Here, indicate whether each material, system or method listed is relevant to your study. If you are not sure if a list item applies to your research, read the appropriate section before selecting a response.

Materials & experimental systems

n/a	Involved in the study
☐	☒ Antibodies
☐	☒ Eukaryotic cell lines
☒	☐ Palaeontology
☐	☒ Animals and other organisms
☒	☐ Human research participants
☒	☐ Clinical data

Methods

n/a	Involved in the study
☒	☐ ChIP-seq
☐	☒ Flow cytometry
☒	☐ MRI-based neuroimaging

Antibodies

Antibodies used	Primary human macrophages were tested for CAR-HER2 expression using a two-step staining protocol: human HER2/ ERBB2 Protein-His tag (Sino Biological Inc, 10004-H08H-100) primary stain followed by Human TruStain FcX (Biolegend, 422302) and Anti-His Tag APC (R&D Systems, IC050A) secondary stain. TruStain FcX (Biolegend, 422302) was always used for FACS staining of monocytes, macrophages, or monocytic cell lines expressing Fc receptors. Macrophage purity was tested using the following panel: Anti-CD11b PE (Biolegend, 301306), Anti-CD14 BV711 (Biolegend, 301838), Anti-CD3 FITC (eBioscience, 11-0038-42), Anti-CD19 PE-CY7 (eBioscience, 25-0198-42), Anti-CD66b PerCP-CY5.5 (Biolegend, 305108), Anti-CD56 BV605 (Biolegend, 318334), and Live/Dead Fixable Aqua (L/D aqua) Dead Cell Stain Kit (ThermoFisher, L34957). The same panel was used for testing the monocyte purity post CD14 MACS selection, prior to seeding for differentiation. M1/M2 markers on primary human macrophages were detected with the following panel: Anti-CD11B PE (Biolegend, 301306), Anti-CD80 BV605 (Biolegend, 305225), Anti-CD86 BV711 (Biolegend, 305440), Anti CD206 BV421 (Biolegend, 321126), Anti CD163 APC-CY7 (Biolegend, 333622), anti HLA-DR BV785 (Biolegend, 307642), Anti-HLA ABC PE/CY7 (Biolegend, 311430) and Live/Dead Fixable Aqua Dead Cell Stain Kit. CD46 expression was detected with Anti-CD46 APC (Biolegend, 352405) and CXADR was detected with Anti-CAR PE (EMD Millipore, FCMAB418PE-I). Appropriate fluorescence matched isotype controls were acquired from Biolegend. Surface HER2 was detected using Anti-Human CD340/HER2 APC (Biolegend, 324408). In phagocytosis assays, macrophages were stained with anti-CD11b APC-CY7 (Biolegend, 301342) and tumor cells, which were all sorted for >99% GFP positivity, were detected on FACS by GFP. The following antibodies were used: human CD4 PerCP/Cy5.5 (BioLegend #344608), human CD8 BV421 (Biolegend #344748), human CD3 BV711 (BioLegend #317328), human CD11b FITC (BioLegend #101206), human CD69 PE (BioLegend #3110906), and L/D Aqua (Thermo). Flow cytometry data were acquired on a BD Fortessa with HTS (BD Biosciences, USA), and analyzed with FlowJo X10 (FlowJo, LLC).
Validation	Antibodies were validated using positive and negative cells or isotype controls. Validation reports were provided by the antibody manufacturers (BioLegend). Appropriate compensation controls were used for every experiment. The BD Fortessa and Attune Nxt were calibrated daily using CS&T beads (BD Biosciences) or manufacturer recommended methods.

Eukaryotic cell lines

Policy information about [cell lines](#)

Cell line source(s)	Cell lines were purchased from and validated by the American Type Culture Collection (ATCC).
Authentication	Cell lines were authenticated as by routine practice by ATCC. Cell lines cultured in-house were validated by ATCC services. Relevant antigen expression was routinely validated during culture.
Mycoplasma contamination	Cell lines were tested for the presence of mycoplasma contamination (MycoAlert™ Mycoplasma Detection Kit, LT07-318, Lonza, Basel, Switzerland). All the cell line were negative for mycoplsma.
Commonly misidentified lines (See [ICLAC](#) register)	None of the cell lines used in this manuscript are listed in the ICLAC Database of Cross-contaminated or Misidentified Cell Lines (Version 8.0).

Animals and other organisms

Policy information about [studies involving animals](#); [ARRIVE guidelines](#) recommended for reporting animal research

Laboratory animals	NOD/SCID Il2rg-/- hIL3-hGMCSF-hSF (NSG-SM3 or NSGS) mice originally obtained from Jackson Laboratories were purchased and bred by the Stem Cell and Xenograft Core at the University of Pennsylvania. Male and female mice were used, age 6-8 weeks.
Wild animals	The study did not involve wild animals.
Field-collected samples	The study did not involve samples collected from the field.
Ethics oversight	All in vivo studies were conducted under IACUC approved protocols under established policies at the University of Pennsylvania.

Note that full information on the approval of the study protocol must also be provided in the manuscript.

Flow Cytometry

Plots

Confirm that:

☒ The axis labels state the marker and fluorochrome used (e.g. CD4-FITC).

☒ The axis scales are clearly visible. Include numbers along axes only for bottom left plot of group (a 'group' is an analysis of identical markers).

☒ All plots are contour plots with outliers or pseudocolor plots.

☒ A numerical value for number of cells or percentage (with statistics) is provided.

Methodology

Sample preparation	Standard flow cytometry protocol was used in this study. Cells were washed before and after staining, and Fc block was used (Human TruStain FcX) when staining Fc receptor expressing cells (macrophages, PBMC's, THP-1s). Samples were acquired on an LSRII Fortessa (BD) or an Attune Nxt using the high-throughput system add-on. Compensation was performed with every experiment and the instrument was calibrated daily using CS&T beads. Sample preparation details on individual experiments are in the Methods section.
Instrument	Flow cytometry was performed on a Fortessa-LSR II cytometer (Becton-Dickinson) or Attune NxT (Thermo Fisher).
Software	FCS files were analyzed with FlowJo X 10.0.7r2 (Tree Star) or later.
Cell population abundance	Target cell lines were sorted for >99% GFP positivity on a BD Influx Cell Sorter (BD Biosciences). THP-1's were sorted for >99% mRFP positivity and >99% CAR positivity on a BD Influx cell sorter by staff at the UPenn Flow Core or the Wistar Flow Core at The Wistar Institute. Purity was determined by flow cytometry during and after the sort. Purity was periodically checked if cells were kept in culture. Primary effector cells were not sorted.
Gating strategy	Generally, FACS gating was performed as follows: FSC/SSC -> Singlets -> Live cells (L/D Aqua negative) -> gating of interest. The appropriate negative control was used for generating gates of interest. For example, for CAR expression, the gate was drawn based on untransduced macrophages that were stained with the same reagents. In other cases, unstimulated macrophages were used to draw the gates of interest, such as in induction of phenotypic markers. In other cases, such as HER2 antigen staining, fluorophore-matched isotype controls were used. For phagocytosis assays, gating was performed as follows: FSC/SSC -> live -> CD11b+ -> CD11b+/GFP+. Gates were drawn using macrophages alone as a control.

☒ Tick this box to confirm that a figure exemplifying the gating strategy is provided in the Supplementary Information.